USING TIME-TO-CONTACT AS A FLIGHT CONTROL PARAMETER TO IMPROVE ROTARY-WING UAS SHIP DECK LANDINGS

Christopher Dadswell, University of Liverpool, Liverpool, UK
Michael Jump, University of Liverpool, Liverpool, UK

Abstract

A vertical landing onto the moving deck of a ship can be challenging even for an experienced aircrew. As interest continues to grow in the use of Uncrewed Aerial Systems (UAS) in military and specifically naval environments, new technologies will be required to improve the safety and reliability of UAS landings at sea. Existing solutions to this are not truly autonomous as they have used infrastructure other than onboard sensors. Tau-Theory is one method proposed to make these vehicles truly autonomous during a deck landing. Tau-Theory seeks to explain how observers guide themselves through the cluttered environment that is the Earth's surface. A simulation environment was created to explore the use of tau, or time-to-contact, as the reference control variable in a feedback control system to land different scales of rotary-wing UAS landing on a moving ship deck. The results of the simulation experiments showed that using tau did provide an advantage over a more conventional descent technique in terms of reduced touchdown velocities if tau could be sensed accurately to the point of touchdown. The developed controller was also agnostic of the vehicle used. However, the passive perception of tau close to the deck became inaccurate when sensed with the gradient methods and visual scene used in this study. Safe touchdowns could still be achieved by the inclusion of an active means to obtain tau during the terminal phase of the descent. The success of the tau-based controller in reducing descent rates was also examined relative to the aircraft's excess heave power available for deck motion at any instant during a landing. As such, a method was developed to help to predict when sufficient control power was available and is presented in this paper.

1. NOTATION

Symbols:

$k, k2, k3$	Tau coupling constants (nd)
q	Electrical charge (C)
t	Instantaneous manoeuvre time (s)
w	Heave velocity (m/s)
x, y, z	Motion gap closure distance (m)
D	Constant of proportionality
K	Control system gain
T	Total manoeuvre time (s)
Z	Heave force stability derivative
δ	Control deflection (???)
τ	Time-to-contact (s)

Dressings:

$\dot{}$	First derivative w.r.t. time
$\ddot{}$	Second derivative w.r.t. time

Subscripts:

c	Pertains to collective
d	Pertains to the ship deck
g	Pertains to a gust
max	Maximum
p	Proportional
ref	Reference value
w	Pertains to a heave velocity
x, y, z	Pertains to motion gap closure distances
G	Pertains to a tau guide
δ_c	Pertains to collective deflection

Acronyms:

ALFURS	Autonomy Levels for Unmanned Rotorcraft Systems
DSTG	Defence Science and Technology Group
FGR	FLIGHTLAB Generic Rotorcraft
RUAS	Rotary-wing Uncrewed Aerial Systems
UAS	Uncrewed Aerial Systems
UCARS	UAS Common Automatic Recovery System

2. INTRODUCTION

The use of Uncrewed Aerial Systems (UAS) has increased dramatically in recent years. Innovations in electrical power systems and aircraft autonomy technologies have driven a significant consumer surge in the use of small UAS. At the same time, there has been a simultaneous increase in both commercial and military use of UAS across a diverse spectrum of aircraft sizes and mission profiles.

The maritime environment is among the most complex mission settings and operations in it pose significant challenges for aircraft. This is true even for pilots of crewed vehicles, especially during launch from and recovery to a ship, discussed in Ref. 1. There are a relatively small number of rotary-wing UAS (RUAS) platforms that exist for this role, in comparison to the number of crewed vehicles in the maritime environment. Those that do, need to be able to operate from ship decks that may be rolling, heaving and pitching. The recently retired Northrop Grumman Fire Scout MQ8 first landed 'autonomously' on an amphibious transport ship in 2006. For such landings, the Fire Scout used a UAS Common Automatic Recovery System (UCARS). UCARS required both a ground tracking station and an aircraft transponder to find the aircraft's relative position to the deck. This information was then relayed to the aircraft by a secure uplink and used to land the aircraft per Ref. 2. The UCARS system was not without its problems. Ref. 3 reports on one mishap where the aircraft had to be forcibly ditched into the sea after repeated problems with the aircraft failing to lock on to the ship-based recovery beacon.

The Autonomy Levels for Unmanned Rotorcraft Systems (ALFURS) Framework of Ref. 4 defines various levels of autonomy ranging from 'Remotely Piloted' (ALFURS = 0) to 'Fully Autonomous' (ALFURS = 10). Although the MQ8 landing capability is described as 'autonomous', the ALFURS scale requires that the platform does not rely on external systems, even for relatively low levels of autonomy. Therefore, to achieve true 'full' autonomy, the aircraft should rely only on sensors that it carries itself to avoid external failures disrupting operational capability. This latter requirement is analogous to the natural world, where flighted animals largely (but not exclusively) rely on sight (i.e. the eyeball) to guide themselves through the cluttered environment close to the Earth's surface.

The University of Liverpool has made significant contributions to the understanding of dynamic ship-helicopter interactions, summarised in Ref. 5, and of how the optical parameter 'tau' (the time to contact an approaching surface) is used for flight control and guidance in crewed aviation. Much of this work is summarised in Ref. 6, but has been extended to, for example, modelling the helicopter autorotation manoeuvre in Ref. 7, modelling of the pilot in Ref. 8 and understanding occupant preferences for landing approaches in Ref. 9.

In this paper, tau is investigated as a guidance parameter to land a RUAS on a moving ship deck, where tau is sensed optically. The ultimate goal here is to provide true 'autonomy' by using sensors onboard the airframe to guide it onto the deck during landing.

The paper is structured as follows. Section 3 introduces Tau Theory and the so-called tau-guides that have been used in this work. Section 4 describes the simulation environment that was created to test tau-based control laws to be used by rotary-wing aircraft to descend to a moving deck. Section 5 presents the results of a study to evaluate the use of the tau-based control algorithms for a moving ship deck scenario for the case where tau is known 'perfectly'. Section 6 then reports on a similar simulation experiment but where tau is being detected 'optically' via a camera model. Finally, Section 7 presents the Conclusions of the study and outlines the planned future work.

3. TAU THEORY

Tau theory has its roots in the ecological approach to psychology and visual perception that was pioneered by Gibson in the mid-20th century and is closely linked to the concepts of optical flow that he proposed in Ref. 10. Gibson's work was developed to examine 'tau' (τ), the instantaneous time-to-contact with an obstacle, by Lee in Ref. 11. Lee hypothesised that humans and animals use this optical-invariant temporal parameter to control and guide purposeful movements.

Tau is simple to compute in spatial terms as the instantaneous ratio between the distance to an obstacle, and the closure rate of the gap between observer and obstacle, Eqn. (1).

$$\tau(t) = \frac{x}{\dot{x}} \tag{1}$$

However, it seems implausible that an observer constantly estimates these parameters and divides one by the other to compute tau if it is to be used as a

guidance parameter. Lee instead considered the apparent motion of the image of the approaching obstacle on a person's retina; the observer could estimate their time-to-contact from the inverse of the apparent rate of expansion of the object in their eye without any conscious cognitive processing.

Lee built on this work in Ref. 12, proposing that the coupling of taus of multiple action gaps was a key element of tau guidance. An action gap is the separation between the current state of a system and a goal state to be achieved through some action. Action gaps are usually a spatial dimension, like the distance between a UAS and a ship deck, but the term can cover a range of other variables that can be sensed e.g., force, pressure etc. This work recognised that gaps often need to be closed synchronously and this can be achieved by coupling the time-to-contacts of multiple action gaps together in some ratio with a coupling constant, as shown in equation (2):

$$\tau_x = k\,\tau_y \tag{2}$$

where 'x' and 'y' are the two sensed gaps to be closed. The value of the constant is between 0 and 1 and can vary depending on task and the system in question.

3.1 Second-Order Intrinsic Tau Guides

Lee conceived of a general intrinsic Tau guide as a time-varying value generated by some bodily process. As it was theorised to be some function of the nervous system, he proposed that this value would be generated by a flow of electric charge from one area of the brain to another, from a full 'reservoir' to an empty one. The rate would be such that the second-order time derivative of the flow was constant. At $t = 0$, the reservoir is full of electrical charge, here termed q_G, and the flow rate is 0. After some time, T_G, the reservoir will be empty. From simple kinematics equation (3) can be constructed to give the amount of charge remaining in the reservoir at some time before emptying.

$$q_G = \frac{1}{2}\ddot{q}_G(T_G^2 - t^2) \tag{3}$$

Again, the value of the Tau guide will be the ratio of distance to close the gap, and gap closure rate. The rate of emptying at a time t will be $-\ddot{q}_G t$, therefore the value of the Tau guide will be:

$$\tau_G = \frac{\frac{1}{2}\ddot{q}_G(T_G^2 - t^2)}{-\ddot{q}_G t} = \frac{1}{2}\frac{t^2 - T_G^2}{t} \tag{4}$$

This expression for the Tau guide can then be coupled to an extrinsic motion gap via the coupling constant, 'k_2':

$$\tau_M = k_2\,\tau_G = \frac{k_2}{2}\frac{t^2 - T_G^2}{t} \tag{5}$$

3.2 Third-Order Intrinsic Tau Guides

Though third-order intrinsic Tau guides have not been explicitly folded into the Tau theory framework, motions that follow their expected movement pattern have been observed in various arm movements. In Ref. 13 Hogan theorised that primates would attempt to minimise jerk (the 3rd order temporal derivative of displacement) during certain voluntary movements to avoid large accelerative transients. He presented a solution to the optimal control problem of forearm motion using a jerk cost function. However, this approach required symmetric velocity profiles that were not always present when performing faster movements.

A later study by Nagasaki examined arm movements over a wide range of speeds and used Hogan's minimum jerk model to analyse the trajectories observed, including an 'asymmetry index' to explain asymmetric velocity profiles that were observed during more aggressive motions [1]. Upon inspection, this index bears immediate similarity to the coupling constants of Tau Theory. There is no literature definitively comparing any natural movement to a defined third-order intrinsic Tau guide, but the equations that such a guide would necessitate are defined in Ref. 14. These third-order guides were derived using the same process as second-order guides, modelling the flow of charge from one area of the brain to another. However, a third-order guide assumes that both $\dot{x} = 0$ and $\ddot{x} = 0$ at $t = 0$, so from simple kinematics the amount of charge left to flow is:

$$q_G = \frac{1}{6}\dddot{q}_G(T_G^3 - t^3) \tag{6}$$

Therefore, the reservoir of charge's time-to-empty is:

$$\tau_G = \frac{q_G}{\dot{q}_G} = \frac{1}{3}\frac{t^3 - T_G^3}{t^2} \tag{7}$$

The guide can then be coupled to an external action gap as usual via k_3:

$$\tau_M = k_3\tau_G = \frac{k_3}{3}\frac{t^3 - T_G^3}{t^2} \tag{8}$$

Third-order intrinsic guides can be useful because they allow for movements with zero acceleration at the start and end of the manoeuvre. First and second-order intrinsic Tau guides necessarily require an instantaneous non-zero acceleration at the start of the manoeuvre, which the controlled system may not be capable of developing, leading to tracking errors.

3.3 Tau Estimation Systems

Estimating time-to-contact is a key task for implementing Tau control and guidance as discussed above. Despite the presentation of several theories, the precise ecological mechanism for sensing time-to-contact remains unclear. A range of approaches have been proposed for electronically estimating time-to-contact. These methods can broadly be divided into two categories: spatial and optical.

3.3.1 Spatial Tau Estimation

A common approach is to calculate time-to-contact from spatial information provided by GPS-INS systems, as reported in Ref. 15. This approach employs aircraft position and velocity estimates to calculate Tau. For example, a descending aircraft's instantaneous time-to-contact with a ground plane using the altitude (z) and descent rate ($\dot{z}$) is simply given by:

$$\tau = \frac{z}{\dot{z}} \tag{9}$$

However, such an approach does not take advantage of some of the advantages of Tau-based guidance, notably their ability to react to changes in the environment. Achieving accurate spatially computed time-to-contact estimates consistently demands comprehensive knowledge of the environment and its dynamics, which is often impractical to collect, store, or utilize. Depending on the source of altitude estimates it is likely that the value is not the true height above terrain, as this would either require an active ranging altimeter, or a database of terrain altitudes in the local area. Terrain database methods are not reactive to dynamic environments, so vulnerable to error. Active ranging instruments such as radar, lidar or ultrasonic sensors are useful prospective tools for Tau estimation, but can be expensive, heavy (not useful for small UAS) or limited in range and resolution.

3.3.2 Optical Tau Estimation

Optical methods offer an alternative by estimating time-to-contact directly from sequences of digital video images without recovering spatial parameters. Passive imaging provides a more obvious analogue to the mechanism used by humans and animals, and optical sensors are low cost and readily available.

Monocular camera-based computer vision is typically unable to recover motion parameters due to scale ambiguity; with only one viewpoint it is impossible to tell the difference between a small object close to the camera, and a larger one further away, Figure 1. However, it is not necessary to recover spatial parameters to compute temporal ones, such as tau. The monocular computer vision schemes examined here can be sub-divided into three further common categories for tau perception: dimension tracking, optical flow divergence, and direct gradient-based methods.

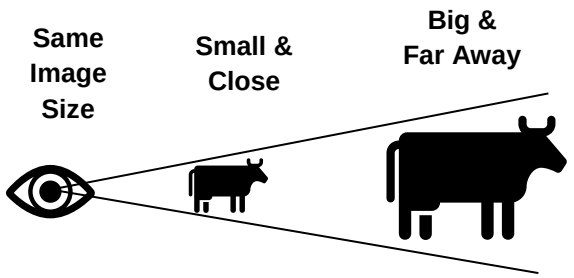

Figure 1: Illustration of scale ambiguity - inability to differentiate between small objects close to a viewpoint, or larger objects further away

Dimension tracking uses size and rate information obtained from a sequence of images to find time-to-contact as described in Ref. 16. While it isn't possible to estimate the true size of an object from only an image of it, the ratio of its apparent size and the rate of change of that size can be used to estimate temporal parameters. Dimension tracking methods are simple and intuitive but performance will degrade in scenarios with rotational motion between observer and target, as rotational motion can skew the apparent size of an object without moving towards or away from it (depending on the dimension(s) being tracked).

A second option for Tau estimation using monocular images stems from the analysis of the optical flow field that develops with camera motion. In a computer vision context, optical flow can be considered the apparent velocity of pixels on the image plane, an example of which is shown in Figure 2. While optical flow methods again do not recover spatial scene parameters, they can yield temporal parameters by analysing the vector flow field, with the divergence of the flow field giving time-to-contact. Optical flow methods can be computationally expensive, and performance

can also be degraded by rotational motion between observer and target. Since rotorcraft must necessarily rotate to translate, this could significantly affect performance of a tau sensor.

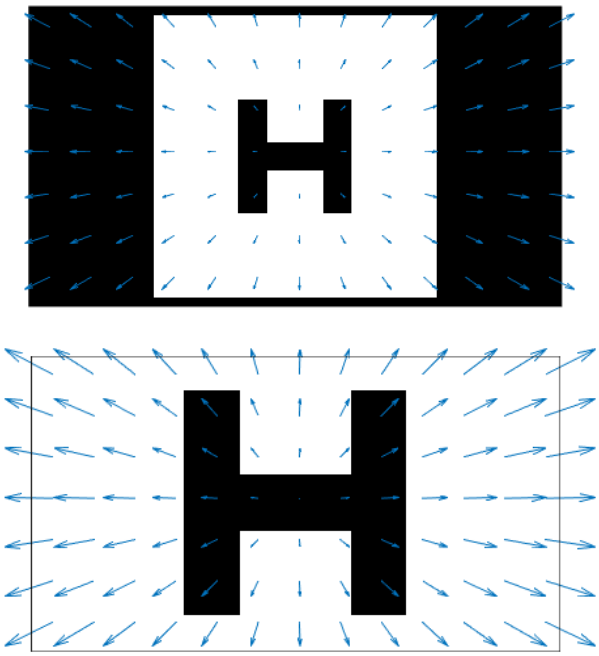

Figure 2: Example of optical flow field components when descending towards a simple representation of a helipad

The third class of methods are known as direct gradient methods and can be considered a synthesis of dimension tracking and optical flow-based methods. Initially proposed by Horn in Ref. 17, a gradient method combines perspective projection equations from dimension tracking and the constant brightness equation of optical flow to simplify the Tau estimation procedure using physical insights to the situation. Horn's work offers three different algorithms for estimating Tau in scenarios of varying complexity, including simple one-dimensional motion, translational motion in three dimensions, and time-to-contact with sloped planar surfaces. A further extension proposed a framework for three-dimensional motion relative to sloped planar surfaces in Ref. 18, and a third extension was proposed in Ref. 19 that incorporates corrections for rotational motion in three dimensions into the method.

Due to the adaptability of direct gradient methods to complex situations with motion in multiple degrees-of-freedom, this method was used to estimate time-to-contact in the deck landings described below, including the extensions for relative slope and motion in 6 degrees of freedom.

More detailed analysis of optical time-to-contact estimation methods, and lessons learned from implementing them, will be presented in future papers.

4. EXPERIMENTAL APPROACH

A virtual scenario was developed to test the efficacy of tau guidance laws, based upon the guides of Section 3, to autonomously land a RUAS on a moving ship deck. Simulation models for each element of the task were created: a camera, a number of different rotorcraft flight dynamics models (including MQ-8B) and a ship helicopter deck. The rotary-wing platforms were tested in a frigate deck landing scenario. The aircraft was always positioned directly over the intended landing spot, making the landing manoeuvre largely a vertical translation. Landings were analysed in a range of sea state conditions up to Sea State 6. Each sea state results in different amounts of deck motion for the aircraft to contend with during landing. Tau estimates from the camera model were used as a feedback control variable to the aircraft model's autopilot to attempt a landing, using the direct gradient estimation method. These were compared with an alternative guidance strategy, which was to approach the deck at a constant vertical speed. It should be noted that the scenario did not include any wind or simulation of the turbulent airwake that would be expected over a ship landing deck, but these factors may be examined in future work.

4.1 Simulation Environment

The Matlab Simulink 3D Animation toolbox provides tools for linking Matlab programs and Simulink models to 3D graphics objects and scenes. Objects defined in standard modelling languages can be positioned within 3D worlds and viewed using virtual cameras. This toolbox provides an easy-to-use set of methods to interface simulation models with a 3D graphics engine. It can be used to generate video for defined camera trajectories or can be integrated into real-time simulations to produce video streams for cameras that move dynamically within a 3D world. These video feeds can then be directly processed using Matlab and Simulink.

A frigate deck landing virtual world was created for use in the simulation experiments. A deck was created using Google Sketchup 3D modelling software and textured with generic deck markings inspired by those found on common UK frigates, shown in Figure 3. Only the landing deck is modelled as the rest of the ship serves no purpose in any of the experiments

described in this paper. The deck was situated in a flat, blue sea. The position of the deck was controlled with inputs to the VR simulation, so deck motion in varying sea states could be easily simulated by coupling the world to a Simulink model. A generic helicopter model from the object library in 3D World Editor was used as a platform for a virtual camera. The parameters of the virtual camera model were set to emulate a camera operating at an HVGA resolution (480 by 320 pixels) at 30 frames per second and the focal length of the camera was 3.04 mm.

The helicopter visual model is not related to the dynamics of the aircraft simulations attached to the virtual world and served only to represent the position and orientation of the vehicle, as well as being a reference for the virtual camera pose. It is not visible in the feed provided by the virtual camera. A view of the frigate deck landing scene is shown in Figure 3.

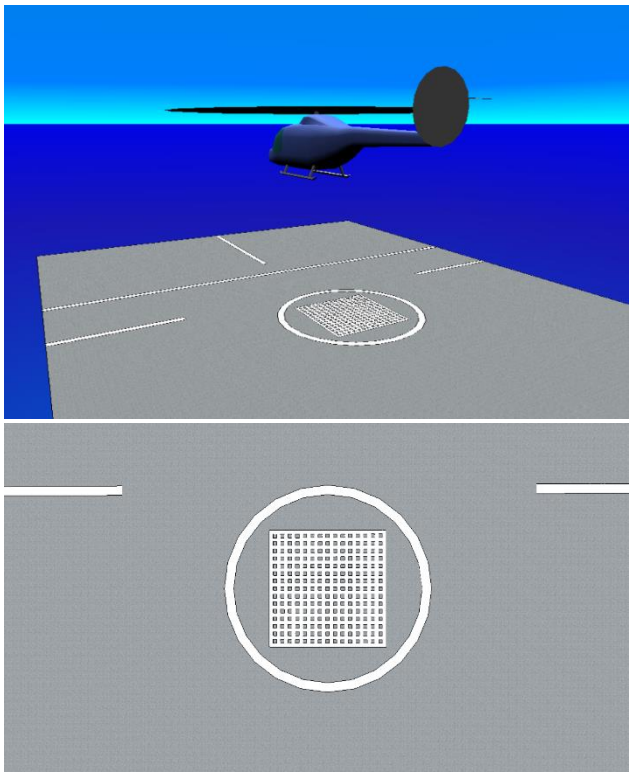

4.2 Figure 3: Frigate deck landing virtual scene developed in Matlab/Simulink 3D Animation toolbox, 3rd person view and downward looking camera view RUAS Flight Models

In order to investigate the efficacy of the Tau control system architecture on a range of aircraft, four rotorcraft flight dynamics models of different aircraft were used. They were all developed in FLIGHTLAB (Ref. 20) during the course of previous projects at UoL. The four rotorcraft models were based upon:

(i) Sikorsky SH-60B 'Seahawk';

(ii) Northrop Grumman MQ-8B 'Fire Scout';

(iii) Yamaha R-MAX and

(iv) Align T-Rex 700.

Each helicopter model makes use of a blade-element model for the main rotor with a three-state Peters-He inflow model, a Bailey rotor model for the tail rotor, and fuselage and empennage aerodynamic look-up tables, illustrated in Figure 4. In addition, the R-MAX and T-Rex models have stability bars which are modelled as a rate feedback gain in the roll and pitch channels.

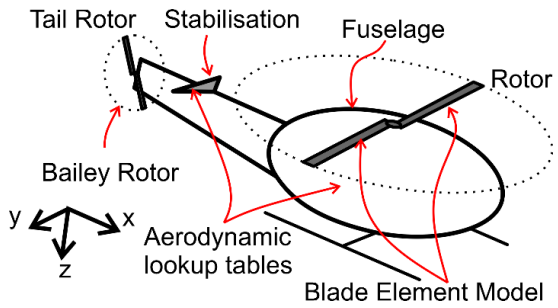

Figure 4: Anatomy of the FLIGHTLAB helicopter models used in the experiment

The Seahawk model, though not typically an unmanned aircraft, is used to represent a human-scale aircraft in the analysis and has been flown autonomously. It was derived from the FLIGHTLAB Generic Rotorcraft Model (FGR), which, in turn, is based on a UH-60A model and is well documented in the literature (Ref. 20). The MQ-8B Fire Scout is an unmanned air and sea support platform based on the Schweizer 333. The FLIGHTLAB model was estimated as a scaled version of the FGR helicopter model to give the same disc-loading as the real aircraft using the main rotor as the scale reference length. The R-MAX is a remotely piloted unmanned helicopter often used in agriculture for crop spraying and as a research platform. The FLIGHTLAB model was developed by DSTG Australia and has had limited internal validation against the on-axis response to controls. The T-Rex 700 is a remotely piloted aerobatic '3D' helicopter. The FLIGHTLAB model for this aircraft was estimated as a scaled version of the R-MAX model and has had limited validation against flight test data provided by the NRC. The salient parameters of these aircraft are displayed in Table 1.

Table 1: Aircraft model key parameters

Aircraft	Rotor Diameter (m)	Mass (kg)	Length (m)
SH60B	16.35	10,400	19.75
MQ-8B	8.4	1,430	7.3
R-MAX	3.115	94	3.63
T-REX	1.582	5.1	1.32

The full non-linear FLIGHTLAB models were linearised to create nine-state linear state-space models of each aircraft for use in Matlab/Simulink. All four aircraft were trimmed in a hover condition at an altitude of 100 ft before being linearised, with no incident wind. These models were then interfaced with the virtual visual environment and the Tau guidance and control system.

4.3 Ship Deck Motion

A physical ground plane was added to all of the rotorcraft simulation models and actuated in order to emulate ship deck motion. Virtual sensors were added to measure its position in relation to the aircraft. Initially, only a single degree of freedom, heave motion in the z-axis, was actuated, but all six degrees of freedom can be actuated for more realistic deck motion. Ship motion profiles were generated in ShipMo3D (Ref. 21) for a generic Type23-like frigate in a variety of sea states to actuate the ship deck. The vertical displacements of the landing deck over thirty seconds for sea states four to six (the example cases used for this study) are plotted in Figure 5.

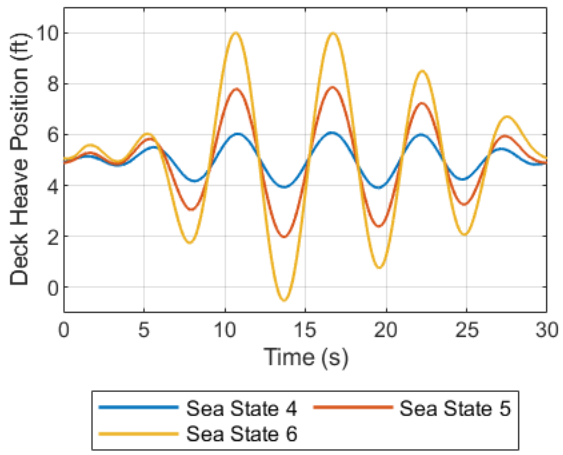

Figure 5: Ship deck heave motion profiles used in the experiment for a range of sea states

The heave motion of the landing deck was found by summing the heave motion of the ship as a whole, and the displacement of the landing deck due to pitch motion. Since the temporal resolution of the data was low compared to that of the aircraft models used, the deck motion data was interpolated using a spline curve to provide smoother data.

4.4 Tau Guidance System

A Tau guidance system was implemented in Simulink and connected to a framework for simulating linear aircraft models. The architecture is independent of any particular aircraft model so that multiple models can be simulated by loading different configuration parameters via a number of setup scripts. Configurations for all the linearised aircraft models described in Section 4.2 were created. The Simulink Virtual Reality toolbox was also integrated into this architecture to allow the generation of virtual camera images for changing aircraft position and orientation in the simulation loop. A simple block diagram of the system architecture is shown in Figure 6.

A tau trajectory generator passed reference values of time-to-contact to the tau controller. The trajectory generator generated second or third-order intrinsic tau guides, each selected by a simple switch. The tau controller only had control authority over the collective control channel of the simulation model. The other channels were controlled by an inner attitude feedback control loop and an outer position control loop. These systems used PID controllers to keep the aircraft hovering over the centre of the ship deck, while holding a constant heading. Tau estimates could be generated from spatial parameters of the aircraft state or estimated from the VR video stream using the direct gradient method described in Section 3.3

The tau controller used a nonlinear ratio control law first proposed for tau control by Kendoul in Ref. 22 and given in Eqn. (10).

$$\delta_C = K_p \left[1 - \frac{\tau_{ref}(t)}{\tau(t)} \right] \tag{10}$$

Tau guidance and control systems must be able to deal with singularities in tau when the relative velocity tends to zero. This tends to rule out traditional proportional feedback control systems that would pass singularities in measured tau to control input directly. Using a ratio between the reference and measured taus means that output should tend towards zero if tau becomes infinite, or 1 when tending towards τ_{ref}.

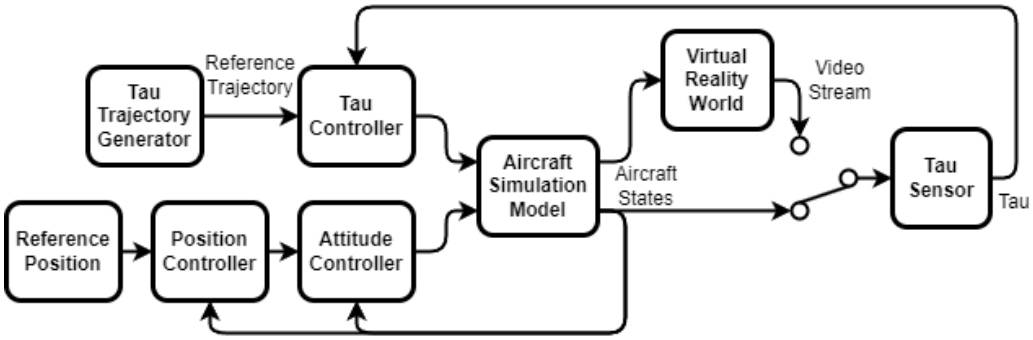

Figure 6: Block diagram of tau guidance system and simulation architecture

5. TAU GUIDED DECK LANDINGS

The Tau guidance system was evaluated in the context of the ship deck landing scenario. Since the Fire Scout was used for operational maritime landings, the MQ-8B linear model was used for the majority of the analyses reported in this paper. The frigate deck VR world was used as the visual scene, and the deck was actuated with the motion from varying sea states. A simple model for collision mechanics was implemented to detect when the landing gear of the aircraft contacted the deck of the frigate, which triggered a switch to update the position of the aircraft in relation to the motion of the ship deck, rather than with the output of the linear model.

Figure 7 shows an example of a tau guided ship deck landing of the M6-8B Fire Scout model in Sea State 4 conditions, following a second order intrinsic tau guide. The initial height above deck is 10m, the manoeuvre duration, $T_G = 10\ s$ and the coupling constant $k_2 = 0.4$. It is compared against a common alternative approach, where the aircraft descends at a constant rate, which reduces by half as the aircraft approaches the deck to reduce touchdown velocity. The aircraft responds to the heaving deck as it descends, accelerating and decelerating to match the motion of the deck as required. This leads to a soft touchdown on the deck with a small relative heave velocity (less than 100 ft/min), which a constant rate strategy could not necessarily achieve. All deck landings discussed in section 5 were performed with spatially computed tau.

The temporal, and therefore spatial, trajectories of an aircraft following a Tau guide can be shaped by varying the type of Tau guide used, the duration of the manoeuvre, and the coupling constant. Variations of these parameters will be explored in the following sections.

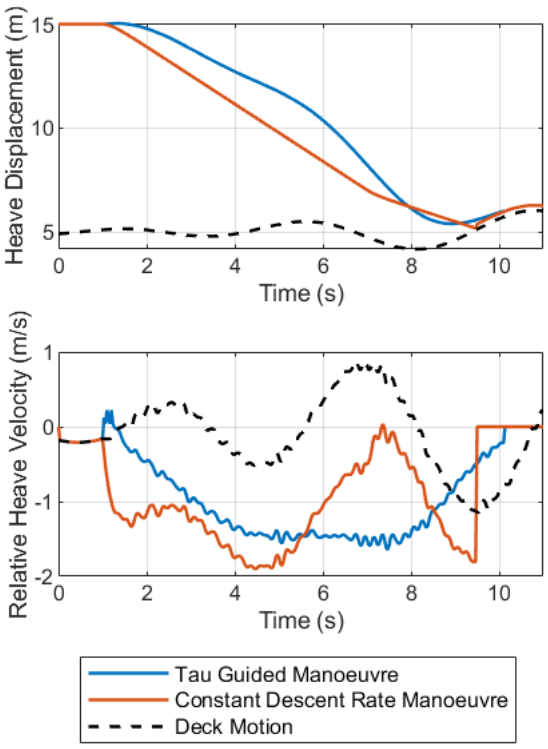

Figure 7: MQ-8B Fire Scout heave dynamics through a simulated Sea State 4 deck landing manoeuvre, guided via tau guidance and constant descent rate guidance

5.1.1 Comparison of Second- and Third-Order Tau Guides

Figure 8 shows the position of the aircraft, and relative velocity between aircraft and ship deck, for two landing manoeuvres performed by the MQ-8B. The aircraft begins in a hover 10 m above the deck and descends vertically, following an intrinsic Tau guide reference trajectory using spatially computed Tau estimates. Both second- and third-order intrinsic Tau guides have been tested here with a coupling constant of $k = 0.4$. A first-order guide has been omitted since the rotorcraft begins at rest, contrary to the assumed initial conditions of a first-order guide. The

deck is actuated with motion calculated for sea state 4. Note the heave velocity of the deck has some low amplitude noise that also manifests in any relative velocity measurements, though this does not seem to significantly affect the overall performance of the system.

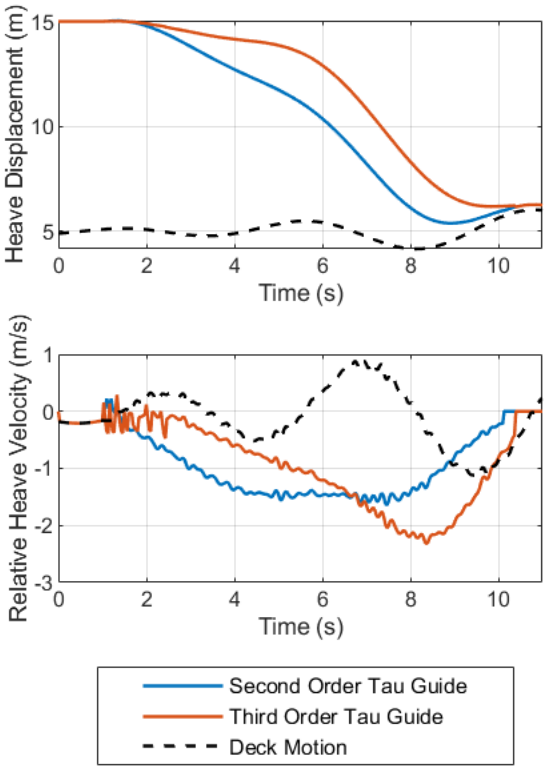

Figure 8: MQ-8B Fire Scout heave dynamics through a simulated Sea State 4 deck landing manoeuvre, guided by 2nd and 3rd order tau guides

The aircraft tracks the motion of the ship deck throughout the manoeuvre to some degree and the relative velocity profiles are of the expected form given by the intrinsic Tau guide equations defined in Sections 3.1 and 3.2. This demonstrates that Tau guidance is reactive to its targeted end point, in this case the ship deck. This is evident when examining the terminal phase of the second-order Tau guide flight; the aircraft descends for the first 9 seconds of the manoeuvre but begins to climb again as the deck of the ship passes through a trough and begins to rise. The distance between the aircraft and deck is still closing, but the aircraft is climbing in the inertial frame to attempt to track the reference value of the time-to-contact, provided to the controller. All of this happens 'automatically', without having to make special provision in the controller.

5.1.2 Comparison of Coupling Constant Variations

The deck tracking behaviour, noted above, can be made more or less evident by tuning the coupling constant, either k_2 or k_3 as illustrated in Figure 9. It is also clear in the $k = 0.5$ Tau guide that the aircraft decelerates as the deck reaches its peak between 5 and 6 seconds, and then accelerates again to catch up as the deck drops. This tuning parameter can hence be used to modify landing behaviour, with high values of k providing early deceleration, and lower values shifting deceleration later in the manoeuvre to suit the needs of the operator, for example; to minimise power requirements.

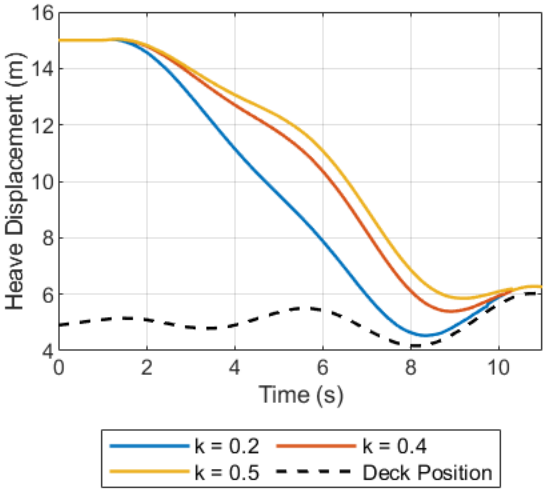

Figure 9: MQ-8B Fire Scout heave displacement through a simulated Sea State 4 deck landing manoeuvre with varying coupling constants

5.2 Predicting Tau Manoeuvre Limits

The results presented thus far indicate that tau guidance may be a useful tool for deck landings, as it is able to deliver consistently low deck touchdown velocities if an accurate tau can be measured. However, it seems likely that there will be some conditions where the aircraft is no longer able to track the heaving deck in high Sea States due to performance limitations of the aircraft, even with accurate estimates of tau. It is possible to provide some insight as to where an aircraft will be unable to perform a particular manoeuvre by leveraging a simple model of rotorcraft heave dynamics from Ref. [2]. This model relates the acceleration of the aircraft to the heave force stability derivatives from a state-space model of a rotorcraft:

$$\dot{w} - Z_w w = Z_{\delta_C}\delta_C + Z_w w_g \tag{11}$$

Where w and $\dot{w}$ are the heave velocity of the aircraft and its time derivative, Z_w is the heave damping stability derivative, $Z_{\delta C}$ is the heave force due to collective deflection, δ_C is collective deflection and w_g is vertical wind gust velocity. In this case, the wind gust can be neglected for simplicity but would be useful to include in further analyses that include the effect of any ship airwake.

The heave velocity, w, and acceleration, $\dot{w}$, required at any time, t, in a tau-guided manoeuvre can be found analytically using the equations presented in Section 2. For a second order intrinsic Tau guide applied to the heave axis, they are:

$$w = -D_\tau \frac{3}{k_2} t^2 (T_G^3 - t^3)^{\frac{1}{k_2}-1} \quad (12)$$

$$\dot{w} = D_\tau \frac{3}{k_2} t \left[\left(\frac{3}{k_2} - 1\right) t^3 - 2T_G^3\right] (T_G^3 - t^3)^{\frac{1}{k_2}-2} \quad (13)$$

Where:

$$D_\tau = \frac{x_0}{T_G^{\frac{2}{k_2}}} \quad (14)$$

Therefore, for the aircraft to be able to follow the guide, the control power must exceed the demands of the manoeuvre:

$$D_\tau \frac{3}{k_2}((t\left[\left(\frac{3}{k_2} - 1\right) t^3 - 2T_G^3\right] (T_G^3 - t^3)^{\frac{1}{k_2}-2} + Z_W(t^2(T_G^3 - t^3)^{\frac{1}{k_2}-1} \leq Z_{\delta_C}\delta_{C_{max}} \quad (15)$$

For this investigation, the SH60B Seahawk state-space model described in Section 4 was examined. The model was generated from the nonlinear FLIGHTLAB model trimmed in a hover, so the stability derivatives are only strictly valid for this condition. The stability derivatives will change with heave velocity but, for this investigation, the assumption was made that this change is small. The heave stability derivatives, therefore, remain constant throughout this analysis. The relevant stability derivatives for the SH60B heave model are $Z_w = -0.0816$, $Z_{\delta_C} = 2.2193$ and the maximum collective deflection from the trim in the hover is $\delta_{C_{max}} = 5.515$. Only positive acceleration is examined here, since for decelerations, the ultimate limiting factor is acceleration due to gravity. For the standard 2nd order Tau guide used throughout this section, $T_G = 10$, $k = 0.4$ and $x_0 = 10\,m$, and these values are used again here. For this Tau manoeuvre the left and right sides of equation (15) are evaluated separately, with the collective control power terms on the right-hand side treated as a threshold that, if breached, will lead to tracking failure during the manoeuvre.

However, if the same manoeuvre is performed over a heaving ship deck, the motion of the ship must also be considered in the model as follows:

$$(\dot{w} + \dot{w}_d) - Z_w(w + w_d) \leq Z_{\delta_C}\delta_C \quad (16)$$

Using the ship deck motion profiles detailed in Section 4.3, the velocity and acceleration profiles were found by taking the first- and second-order gradients of the heave displacement, and added to the Tau guide acceleration demands for several sea states. Since it isn't immediately clear where the maximums of this function lie, they were calculated across the Tau manoeuvre duration and the whole envelope of the ship deck motion profile and rendered as a 3D surface. The accelerative demands for a sea state four landing, and control power threshold, are plotted in Figure 10.

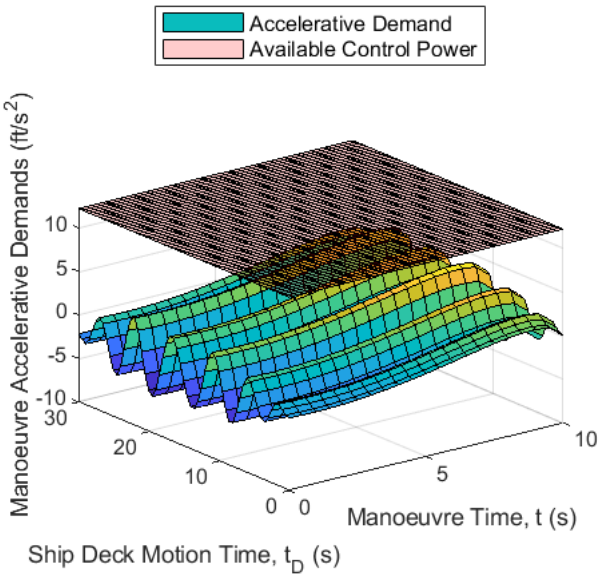

Figure 10: Heave acceleration required and available for an SH60B to perform an ideal second-order tau guided vertical landing on a heaving ship deck in Sea State 4 conditions

The acceleration does not approach the available control power and there is a significant margin in this sea state 4 example, but the motion of the deck is clearly reflected in the acceleration required throughout the manoeuvre.

Figure 11 shows the accelerative demands of a Sea State 6 deck landing, and the available acceleration of the SH60B. In this scenario, the Seahawk

helicopter is not able to produce enough heave acceleration to match the demand of the Tau guide and deck motion combined in certain regions of the operational space. Therefore, the aircraft is not able to track the Tau guide at these points. If these regions occur during the terminal phase of the manoeuvre as the aircraft nears the deck, it will likely hit the deck with a higher velocity than planned or desired. On the other hand, if the aircraft can touch down between these points, there is still a large enough margin to complete the manoeuvre with a low touchdown velocity.

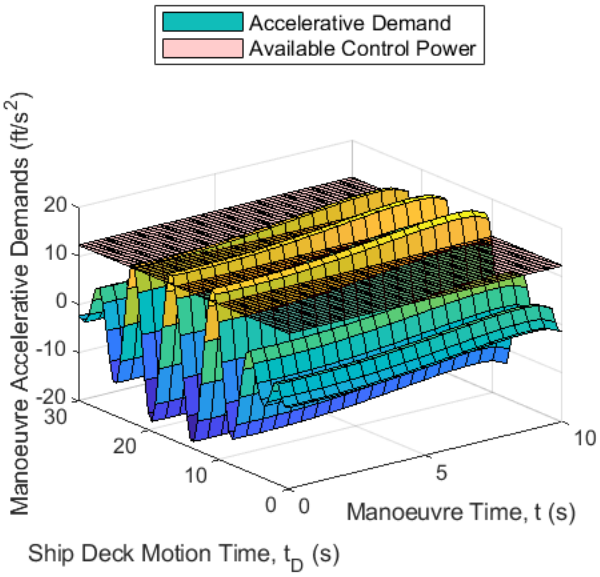

Figure 11: Heave acceleration required and available for an SH60B to perform an ideal second-order tau guided vertical landing on a heaving ship deck in Sea State 6 conditions

To test the hypothesis that this analysis technique can be used to predict the performance limits of an aircraft, the SH60B was investigated using the same start point variation experiment applied to the MQ-8B earlier. The two other aircraft models, the R-Max and T-Rex, were also used to demonstrate a range of aircraft at different scales using Tau guidance. The Fire Scout is included again for the sake of comparison. Figure 12 shows each of the four aircraft undertaking the same second-order Tau guide landing on a ship deck in sea state 4, with ten different start points evaluated. The deck motion at the expected end point is also plotted.

All four aircraft are able to follow the Tau guide and land with a touchdown velocity of less than 1 m/s or 200 ft/min at all points through the deck motion profile. No parameters were changed in the Tau controller, which demonstrates that this control method is essentially platform independent; it is equally applicable to all four aircraft and can deliver similar performance if the heave control power of the aircraft is sufficient.

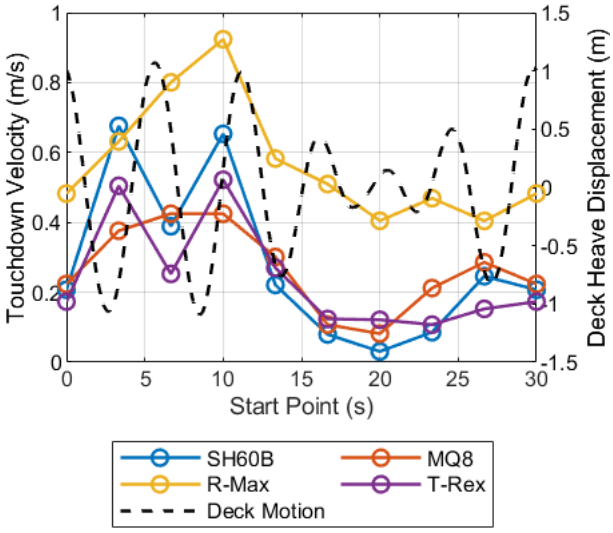

Figure 12: Touchdown velocity for sea state 4 deck landings using a second-order intrinsic Tau guide for four different aircraft

The R-Max, the aircraft with the worst heave control power, exhibits slightly higher touchdown velocities throughout the deck motion profile, even at this relatively low sea state. On the other hand, the SH60B exhibits touchdown velocities below 150 ft/min throughout, but it does increase slightly through points of deck upswing.

Figure 13 shows the same analysis for sea state 6 deck motion. Again, the R-Max experienced high touchdown velocities due to its low vertical control power. As predicted during the previous analysis, the SH60B is also not able to track the deck motion through areas of high deck upswing, and lands heavily. As a result, it can be concluded that the modelling technique proposed above can be used for indication of the performance limits of rotorcraft performing Tau deck landings, though further analysis with nonlinear flight models is required to validate this conclusion.

The order of the aircraft from highest to lowest touchdown velocity is not consistent at all test points, especially when the point of touchdown does not coincide with a deck upswing in the time history. For example, the best performer out of the MQ8 and T-Rex switches at each of the first 4 test points, depending on how the deck is moving. This suggests that there are more factors in the determination of Tau landing performance than purely heave control power. This

variability may be due to a range of handling qualities considerations or control system tuning problems and warrants further investigation.

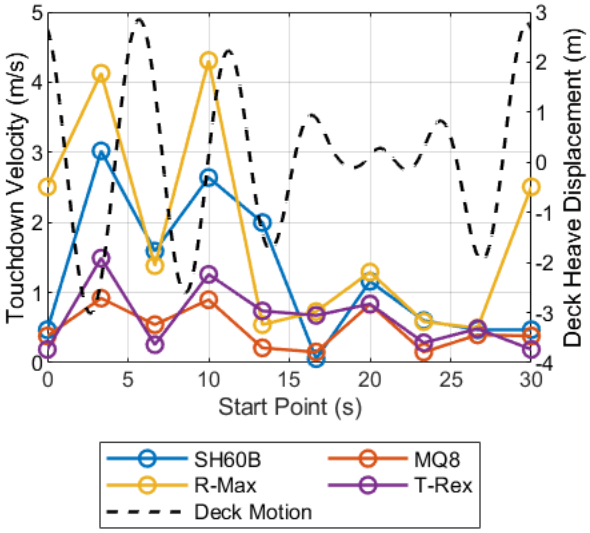

Figure 13: Touchdown velocity for sea state 6 deck landings using a second-order intrinsic Tau guide for four different aircraft

6. OPTICAL TAU GUIDED DECK LANDINGS

The deck landings presented to this point have used spatially computed values of tau relative to the moving deck, which is 'perfect' knowledge of tau. This has demonstrated the possible benefits of tau guidance in this situation, specifically the ability of the guidance system to react to a dynamic landing platform without outside input required. However, a real-world implementation of a tau guidance system must perceive tau and be able to usefully apply the resulting estimate, whilst coping with, for example, sensor noise, imperfect tau perception etc. This Section presents the results of simulated deck landings where tau is 'sensed' using the optical camera model.

The system was initially evaluated using Sea State 1 deck motion conditions, which corresponds to a flat, calm ocean with no heave displacement of the deck. The Tau reference trajectory, measured Tau value, and the ground truth value are shown in Figure 14 for the MQ-8B model following a second-order intrinsic Tau guide.

The measured value of Tau is the one used by the controller to generate the error signal to generate control inputs, equivalent to the tracking error plotted above in Figure 14. The tracking performance is very good between 4 and 9 seconds, with an error consistently below 0.5 seconds except for some small discontinuities.

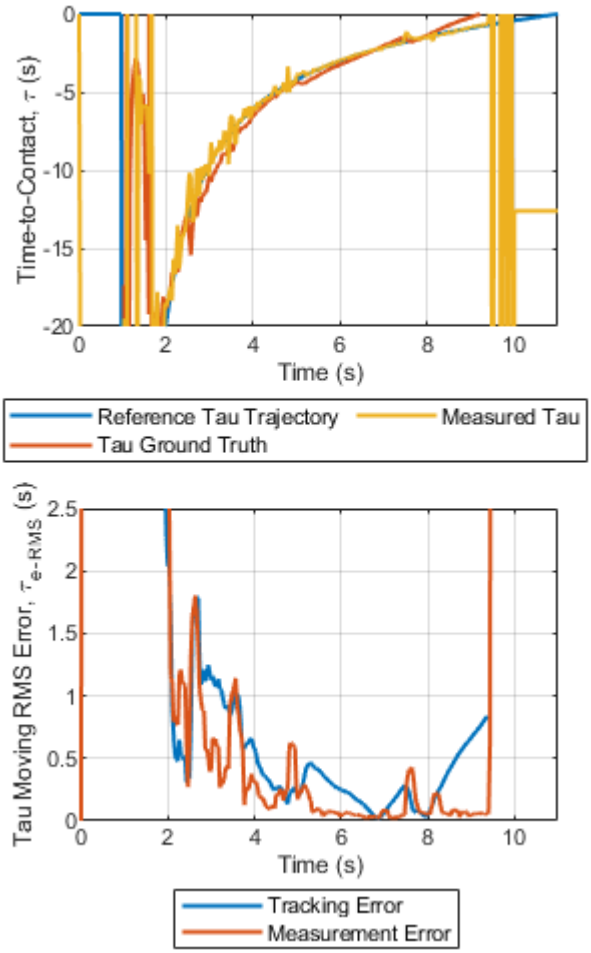

Figure 14: Tau quantities through an optical Tau guided ship deck landing by the MQ-8B in Sea State 1.

There are larger errors in the first 3 seconds of the manoeuvre, but this is unsurprising since the value of the reference trajectory is high and changes quickly at this point. It is also not problematic since the aircraft is a long way from the deck at this point. The error between the measured value of Tau and the ground true value is also low between 4 and 8 seconds but begins to increase rapidly after 8 seconds as the estimated value becomes larger than the true value.

This increase in estimated tau value should result in an acceleration toward the deck, and this is observed by the heave displacement and relative velocity plotted in Figure 15; instead of decelerating at the end of the manoeuvre, the measurement error causes the aircraft to remain at a high velocity and contacts the deck with a vertical speed of 1.3 m/s. The high error at the beginning of the manoeuvre also seems to cause a large spike in velocity as the aircraft begins to descend.

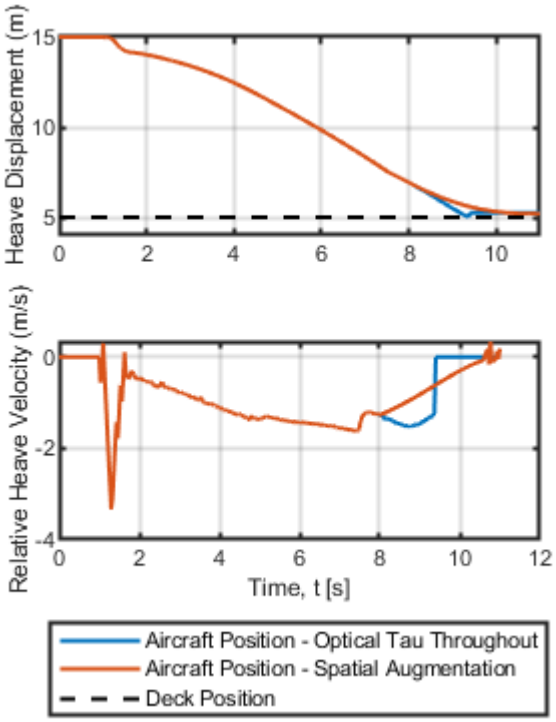

Figure 15: MQ-8B Fire Scout heave dynamics through a simulated Sea State 1 deck landing manoeuvre, following a 2nd order Tau guide using optically sensed tau estimates

Analysis of the direct gradient method suggested that there would be small errors as the camera approached the deck, but it was not clear that it would be this significant. It does not seem possible to mitigate for these problems simply with the available techniques. As a result, it is suggested, that, for this particular experimental configuration, that optical Tau perception is not suitable for the terminal phase of this deck landing manoeuvre. It is proposed that performance could be augmented with an active tau sensor for improved performance. Since this divergence in measurement occurs in the last 2m of descent, an ultrasonic sensor could be used effectively for this situation. This solution was implemented in simulation, with Tau measured from the optical camera feed through the first 7 seconds of the Tau manoeuvre, and then switched to a spatial estimate calculated using the aircraft height above the deck and relative velocity. Figure 15 also shows the same descent carried out with this switch to a spatial Tau estimate for the final 3 seconds of the descent.

Optical Tau guided landings were also performed with higher sea state motion. Figure 16 shows the same second-order Tau guided descent by the Fire Scout onto a deck moving in Sea State 3 conditions. Again, the augmentation with spatial data is used for the final 3 seconds of the manoeuvre. The aircraft is able to make a 'soft' landing on the deck with only a small relative velocity of less than 100 ft/min.

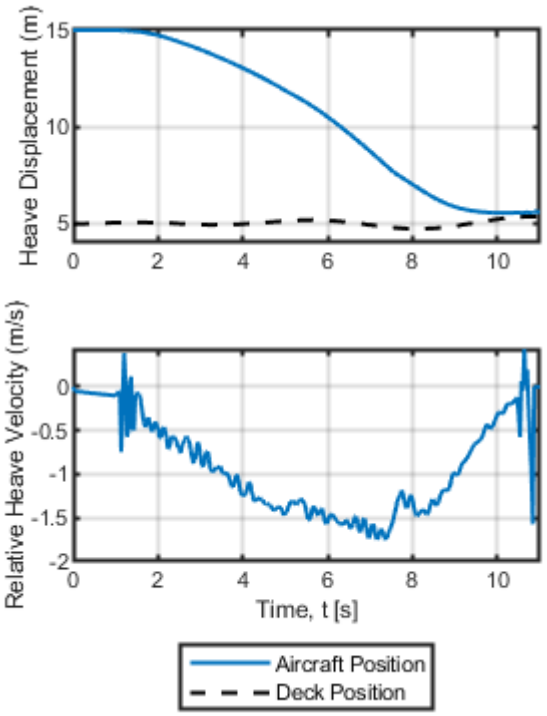

Figure 16: MQ-8B Fire Scout heave dynamics through a simulated Sea State 3 deck landing manoeuvre, following a 2nd order Tau guide using optically sensed tau estimates augmented with spatial estimates in the terminal phase

The deck motion for Sea State 3 is still relatively benign, so the results for the same experiment performed in Sea State 5 are plotted in Figure 16. This descent gives a much better view of how optically perceived Tau can still be a powerful tool in this scenario, as the aircraft clearly slows its descent to avoid the peak in deck position 5 seconds into the manoeuvre. This is accomplished using only optical Tau as a control variable, and occurs at a range where an ultrasonic ranging sensor would not be accurate, though it is still necessary to augment the optical Tau estimate with a spatial one through the final phase of the landing.

The descent in Figure 16 again exhibits the large transient velocity after manoeuvre initiation, which is undesirable. Since third-order intrinsic Tau guides should start with zero acceleration and develop velocity more slowly, they may offer a mechanism for reducing this velocity spike.

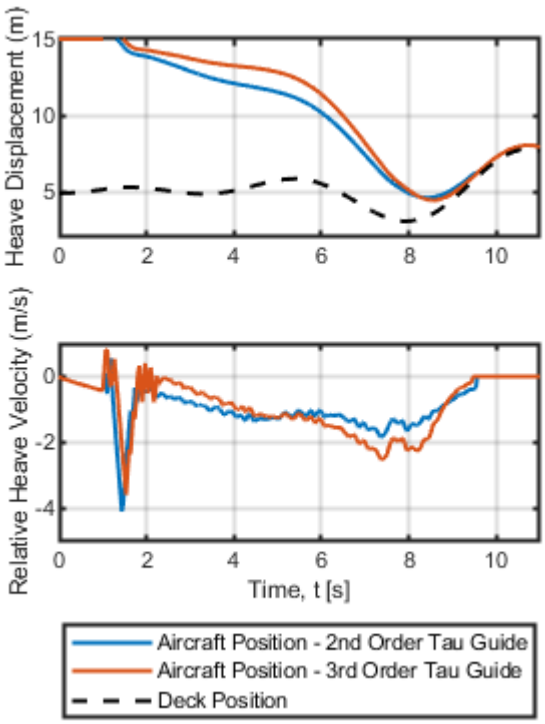

Figure 16: MQ-8B Fire Scout heave dynamics through a simulated Sea State 5 deck landing manoeuvre, following 2nd and 3rd order Tau guides using optically sensed tau estimates augmented with spatial estimates in the terminal phase

Figure 16 also shows the heave dynamics for an optically guided third-order Tau descent in sea state 5. Spatial Tau augmentation is again used over the final 3 seconds of the manoeuvre. Unfortunately, following a third-order intrinsic Tau guide does not reduce the velocity spike that occurs during manoeuvre initiation, as was thought. This seems to be because the reference Tau trajectory is similar to a second-order guide in that they both produce a reference Tau of negative infinity at the start of the reference trajectory, which despite saturation functions being included, is still partially transmitted to the controller. If the deck was stationary then the measured value of Tau would also be infinite and this would not be a problem, but since the deck continuously heaves relative to the aircraft, a non-infinite value of Tau is measured and this leads to a large error signal being passed to the controller. Nevertheless, the velocity spike does not result in a large displacement, so should not pose a large risk to the safety of the aircraft, and it is likely this transient would be possible to filter out with additional development beyond the scope of this paper.

7. CONCLUSIONS AND FUTURE WORK

A simulation study has been conducted to ascertain the efficacy of the use of time-to-contact (or tau) as a reference control variable to assist with rotorcraft vertical descents to a moving ship deck. The following can be concluded from the investigation:

- When tau is detected accurately throughout a manoeuvre, the proposed simple control algorithm yields a useful means to bring the rotorcraft into contact with the deck surface at safe descent rates. The algorithm tracks the motion of the deck and, provided that the rotorcraft has sufficient control power, will cause the vehicle to synchronise with that motion prior to touchdown.
- A heave analysis technique successfully predicts when the vehicle will run out of control power to be able to successfully follow the deck motion.
- The ‘aggression’ of the control algorithm i.e., how closely it follows the deck motion, could be tuned with a single coupling parameter. However, once tuned, the controller is agnostic to vehicle type, size, dimensions etc.
- When tau was detected using a monocular camera model, the estimates that were produced for tau were useable until the terminal phase of the manoeuvre. With the current modelled environment, purely passive means of tau detection would therefore not be possible to achieve the deck landing. Augmentation using (simulated) active means for the final phase of the descent meant that safe touchdowns could still be achieved.

During the course of this investigation, a number of different tau perception methods were investigated. The Direct Gradient Method has been reported in this paper but the results achieved and lessons learned from utilising the other methods will be reported in future papers. The results reported used a single outside world visual scene, picked to be representative of a typical landing deck. However, the tau perception methods used may be more effective if different deck markings are used and this will form part of a future study. There are also other techniques e.g., scheduled image sub-sampling, that may improve the passively detected tau estimates during the terminal phase of the descent manoeuvre and these will be investigated in the future. Finally, once a configuration has been selected using simulation to give useable

guidance all of the way down to the deck (ideally passively), this will be replicated in a laboratory environment to try to prove the concept in hardware.

Author contacts:

Dr. Chris Dadswell c.m.dadswell@liverpool.ac.uk
Prof. Michael Jump mjump1@liverpool.ac.uk

8. ACKNOWLEDGMENTS

The authors gratefully thank the University of Liverpool's Faculty of Science & Engineering who provided match funding for the UK's Engineering & Physical Science research Council's grant EP/J013714/1 to make this research possible. The authors would also like to acknowledge DSTG Australia and NRC in Canada for the provision of the R-MAX and T-REX nonlinear rotorcraft models. The authors also thank Professor Mark White and Dr Vincent Page of the University of Liverpool for their advice on this paper.

9. REFERENCES

1. T.R.Fell, M.D. White, M. Jump, I. Owen, and S. Manso. Sensitivity Study Of A Small Maritime Rotary UAS Operating In A Turbulent Airwake. Presented at the 71st AHS Forum, Virginia Beach, VA, 2015.
2. Ferrier, B. de, Sehgal, A. K., and Ernst, R. FIRE SCOUT UAV LAUNCH AND RECOVERY SYSTEM PERFORMANCE IMPROVEMENT. 2014
3. Zach Rosenberg. Fire Scout Flights Suspended Due to Crashes. Flight Global, Apr 09, 2012.
4. Kendoul, F. "Survey of Advances in Guidance, Navigation, and Control of Unmanned Rotorcraft Systems." *Journal of Field Robotics*, Vol. 29, No. 2, 2012, pp. 315–378. https://doi.org/10.1002/rob.20414.
5. Owen, Ieuan & White, Mark & Padfield, Gareth & Hodge, S.J. (2017). A virtual engineering approach to the ship-helicopter dynamic interface - A decade of modelling and simulation research at the University of Liverpool. The Aeronautical Journal. 121. 1-25. 10.1017/aer.2017.102.
6. Padfield, G. D. "The Tau of Flight Control." *The Aeronautical Journal*, Vol. 115, No. Journal Article, 2016, pp. 521–556.
7. Alam, M., Jump, Michael, and Cameron, Neil. Can Time-To-Contact Be Used To Model A Helicopter Autorotation? Presented at the 8th Asian/Australian Rotorcraft Forum, Ankara, Turkey, 2019
8. Lu, L., Jump, M., and Padfield, G. D. "Development of a Generic Time-to-Contact Pilot Guidance Model." *AIAA Journal of Guidance, Dynamics and Control*, No. Journal Article, 2017, p. 12. https://doi.org/10.2514/1.G003135
9. u, L., Jump, M., White, M. D., and Perfect, P. "Development of Occupant-Preferred Landing Profiles for Personal Aerial Vehicles." *AIAA Journal of Guidance, Dynamics and Control*, Vol. 39, No. 8, 2016, pp. 1805–1819. https://doi.org/10.2514/1.G001608.
10. Ref. Gibson, J. J. (1979). *The Ecological Approach to Visual Perception*. Boston: Houghton Mifflin
11. Lee, D. N. (1976). A Theory of Visual Control of Braking Based on Information about Time-to-Collision. Perception, 5(4), 437–459. https://doi.org/10.1068/p050437
12. David N. Lee (1998) Guiding Movement by Coupling Taus, Ecological Psychology, 10:3-4, 221-250, DOI: 10.1080/10407413.1998.9652683
13. Hogan N. (1984). An organizing principle for a class of voluntary movements. *The Journal of Neuroscience : the official journal of the Society for Neuroscience*, *4*(11), 2745–2754. https://doi.org/10.1523/JNEUROSCI.04-11-02745.1984
14. H. Nagasaki, "Assymetric velocity and acceleration profiles of human arm movement," *Experimental Brain Research,* vol. 74, pp. 319-326, 1989.
15. Z. Zhang, S. Zhang, P. Xie and O. Ma, "Bio-Inspired 4D Trajectory Generation for UAS Rapid Point-to-Point Movement," *Journal of Bionic Engineering,* vol. 11, no. 1, pp. 72-81, 2014.
16. B. K. Horn, *Robot Vision,* Boston: MIT Press, 1986.
17. B. K. Horn, Y. Fang and I. Masaki, "Time to Contact Relative to a Planar Surface," in *IEEE Intelligent Vehicles Symposium*, Istanbul, Turkey, 2007.
18. B. K. Horn, Y. Fang and I. Masaki, "Hierarchical Framework for Direct Gradient-Based Time-to-Contact Estimation," in *IEEE Intelligent Vehicles Symposium*, Xi'an, China, 2009.
19. H. Zhang and J. Zhao, "Biologically Inspired Vision Based Control Using Featureless Time-to-Contact Estimation," in *IEEE International Conference on Advanced Intelligent Mechatronics*, Banff, Canada, 2016.
20. Du Val, R. W., and He, C. "Validation of the FLIGHTLAB Virtual Engineering Toolset." Aeronautical journal, Vol. 122, No. 1250, 2018, pp. 519–555. https://doi.org/10.1017/aer.2018.12.
21. DSA, "ShipMo3D," DSA, 2019. [Online]. Available: https://dsa-ltd.ca/shipmo3d/overview/.

22. F. Kendoul, “Four-Dimensional Guidance and Control of Movement Using Time-to-Contact: Application to Automated Docking and Landing of Unmanned Rotorcraft Systems,” *International Journal of Robotics Research,* vol. 33, no. 2, pp. 237-267, 2013.